applied sciences

MDPI

Article

High temperature (up to 950 °C) sensor based on micro taper in-line fiber Mach-Zehnder interferometer (Invited)

Yun-Cheng Liao[1,2], Bin Liu[1,2*], Juan Liu[1,2], Sheng-Peng Wan[1,2], Xing-Dao He[1,2], Jinhui Yuan[3], Xinyu Fan[4] and Qiang Wu[5]**

[1] Key Laboratory of Nondestructive Test (Ministry of Education), Nanchang Hangkong University, Nanchang 330063, China
[2] National Engineering Laboratory for Destructive Testing and Optoelectronic Sensing Technology and Application, Nanchang HangKong University, Nanchang 330063, China
[3] State Key Laboratory of Information Photonics and Optical Communications, Beijing University of Posts and Telecommunications, Beijing, China
[4] State Key Lab Adv Opt Commun Syst & Networks, Shanghai Jiao Tong University, 800 Dongchuan Rd, Shanghai 200240, Peoples R China
[5] Faculty of Engineering and Environment, Northumbria University, Newcastle Upon Tyne, NE1 8ST, United Kingdom
* Correspondence author: liubin_d@126.com
** Correspondence author: qiang.wu@northumbria.ac.uk

Featured Application: The sensor developed in the paper can be used for high sensitivity temperature detection of power system, biomedicine, aerospace, and so on.

Abstract: A high temperature (up to 950 °C) sensor was proposed and demonstrated based on a micro taper in-line fiber Mach-Zehnder interferometer (MZI) structure. The fiber MZI structure comprises a single mode fiber (SMF) with two micro tapers along its longitudinal direction. Annealing at 1000 °C was applied to the fiber sensor to stabilize the temperature measurement. The experimental results showed that the sensitivity was 0.114 nm/°C and 0.116 nm/°C for heating and cooling cycle, respectively, and, after two days the sensor still has sensitivity of 0.11 nm/°C, showing good stability of the sensor. An probe-type fiber MZI is designed by cutting the sandwiched SMF, which has good linear temperature responses of 0.113 nm/°C over large temperature range from 89 °C to 950 °C. The probe-type fiber MZI temperature sensor is independent to the surrounding RI and immunity to strain. The developed sensor has a wide application prospect in the fields of high temperature hot gas flow and oil and gas field development.

Keywords: optical fiber; Mach-Zehnder interferometer; high-temperature sensor;

1. Introduction

Optical fiber interferometer sensors have advantages of small size, compact and high sensitivity, which are widely used in petroleum, chemical industry physical and biomedicine sensing [1–5]. There are various types of optical fiber interferometers, including fiber Fabry-perot interferometer, Mach-Zehnder interferometer (MZI), Michelson and Sagnac interferometer [6-15]. Among these sensor structures, optical fiber MZI sensor has attracted considerable research interest and been applied for various parameter measurements, such as temperature, strain, bending, liquid level, and refractive index (RI) due to its flexibility in structure design [16-23]. Single mode-multimode-single mode (SMS) fiber structure is a typical fiber inline MZI configuration, where the multimode fiber (MMF) section could be multimode fiber [24], photonic crystal fiber [25], thin-core fiber [26-28], no-core fiber and twin/multiple core fiber [29-33]. These structures are based on the fusion splicing between two single mode fibers (SMFs) and a multimode fiber section. Once the MMF section is given, very limited flexible design of the sensor can be provided.

In this paper, a novel in-line fiber MZI sensor based on micro taper structure was proposed and investigated in both theoretical and experimental studies. The structure is based on a single SMF, where two micro tapers are created with a short SMF sandwiched between the two micro tapers. The first micro taper is to excite multiple modes transmitting within both the core and cladding of the sandwiched SMF and the second micro taper is to collect these multiple modes into the output SMF. Since the micro taper can be created using common commercial fusion splicer, the structure of micro taper is flexible simply by controlling the arc-discharge parameters, such as arc-discharged time, power, and stepped length, resulting in different coupling coefficients from input SMF to sandwiched SMF, and thus a flexible design of the sensor structure. To demonstrate the application of the micro taper design, a high-temperature measurement (up to 950 °C) was studied experimentally. In addition, to demonstrate the practical application of the sensor, a probe-typed fiber MZI by cutting the sandwiched SMF was studied for high temperature measurement.

2. Theoretical Analysis and Simulations

2.1 Theoretical Analysis

A schematic diagram of the micro taper in-line fiber MZI is shown in Fig.1.

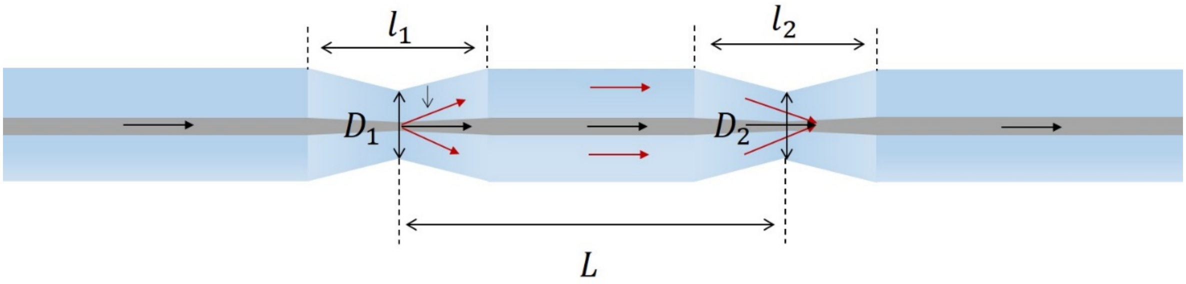

Figure 1. Schematic diagram of the micro taper in-line Fiber MZI.

In Fig. 1, L is the length of the sandwiched SMF between two taper waists of the sensor, l_1 and l_2 are the length of micro taper, while D_1 and D_2 are the waist diameter of micro taper. Light is injected from broadband source into the input SMF transmitted in the core of SMF. In the taper section, since the taper is not adiabatic, the light in the core of SMF will excite cladding modes and these modes together with core mode will transmit independently within both core and cladding of the sandwiched SMF between the two tapers (D_1 and D_2). Since these modes have different propagation constant, when they recouple into the output SMF at the second taper D_2, interference between these modes will take place, resulting in power variations. The intensity of the output of the proposed MZI owing to the interference between the core mode and ith order cladding mode is:

$$I_T = I_1 + I_2 + 2\sqrt{I_1 I_2}\cos(\Delta\varphi) \qquad (1)$$

where I_1 and I_2 are the light intensities of the core and ith cladding modes, and $\Delta\varphi$ is the phase difference between them. Assuming L is the length of the sandwiched SMF between two taper waists and λ is the input wavelength, the phase $\Delta\varphi$ can be expressed as below:

$$\Delta\varphi = 2\pi \frac{(n_{co} - n_{cl})L}{\lambda} \qquad (2)$$

where n_{co} and n_{cl} are the effective refractive indexes of the core and cladding, respectively. The free spectral range (FSR) of the fabricated MZI can be expressed as:

$$\text{FSR}=\frac{\lambda^2}{(n_{co}-n_{cl})L} \tag{3}$$

The FSR is inversely proportional to the interaction length, and the wavelength with minimum output light intensity are located at:

$$\lambda_{dip}=\frac{2}{2m+1}(n_{co}-n_{cl})L \tag{4}$$

Where m=0, 1, 2… When the surrounding temperature of the fiber changes, the sensitivity of the sensor can be expressed as:

$$\frac{d\lambda}{dT}\approx\frac{\left[\frac{\lambda}{\Delta n_{eff}^m}\left(\frac{\partial\Delta n_{eff}^m}{\partial n_{co}}\frac{dn_{co}}{dT}+\frac{\partial\Delta n_{eff}^m}{\partial n_{cl}}\frac{dn_{cl}}{dT}\right)+\frac{\lambda dL}{LdT}\right]}{1-\frac{\lambda}{\Delta n_{eff}^m}\frac{\partial\Delta n_{eff}^m}{\lambda}} \tag{5}$$

where Δn_{eff}^m is the effective refractive index (RI) difference between the core and m[th] cladding mode.

2.2 Simulations

Based on the above theoretical analysis, the fiber-optic sensor was numerically simulated using the beam propagation method (BPM). The simulate conditions are based on a 2D model with mesh size in the X and Z directions of 0.1 μm and 1 μm respectively, and the boundary condition adopted a perfectly matched layer (PML) condition in the model. SMF core and cladding diameters are 8.2 μm and 125 μm, and the corresponding RIs are 1.4682 and 1.4628 respectively. The length (l_1=l_2) and taper diameter (D_1=D_2) of micro taper fiber were set as 500 μm and 80 μm respectively. The simulated transmission spectra have length *L*=1, 2, and 3 cm and a wavelength range of 1540 nm to 1600 nm as shown in Fig. 2(a), and the corresponding spatial spectrogram calculated with Fast Fourier Transform (FFT) were shown in Fig. 2(b). Figures 2(c) and (d) show distributions of the optical field propagating along the MZI and the corresponding normalized optical intensity change at dip A and peak B, respectively. The spatial spectrum ε relationship is [34]:

$$\varepsilon=\Delta m_{eff}L/\lambda^2,\qquad \Delta m_{eff}=\Delta n_{eff}-\lambda_0\frac{\partial}{\partial\lambda}\Delta n_{eff} \tag{6}$$

Where Δn_{eff} is the effective RI difference due to the inter-mode dispersion, and Δm_{eff} indicate the effective RI difference caused by inter-mode dispersion. When the center wavelength λ is a constant, the spatial spectrum is proportional to the effective RI difference Δm_{eff} and the interference length. As can be seen from Fig. 2(b), for all the three *L*, there are several peaks in the MZI spatial spectrum, indicating that there are multiple modes participating and interfering each other. A main peak (exclude the frequency 0) whose amplitude is much larger than other small peaks can be observed, and the spatial frequency increases as *L* increases. Since the high-order cladding mode corresponds to a higher spatial frequency, the low-order cladding mode dominates the inter-mode interference as shown in Fig. 2(b). Therefore, it is reasonable to assume that the MZI is mainly caused by interference between excited low-order cladding mode and core mode.

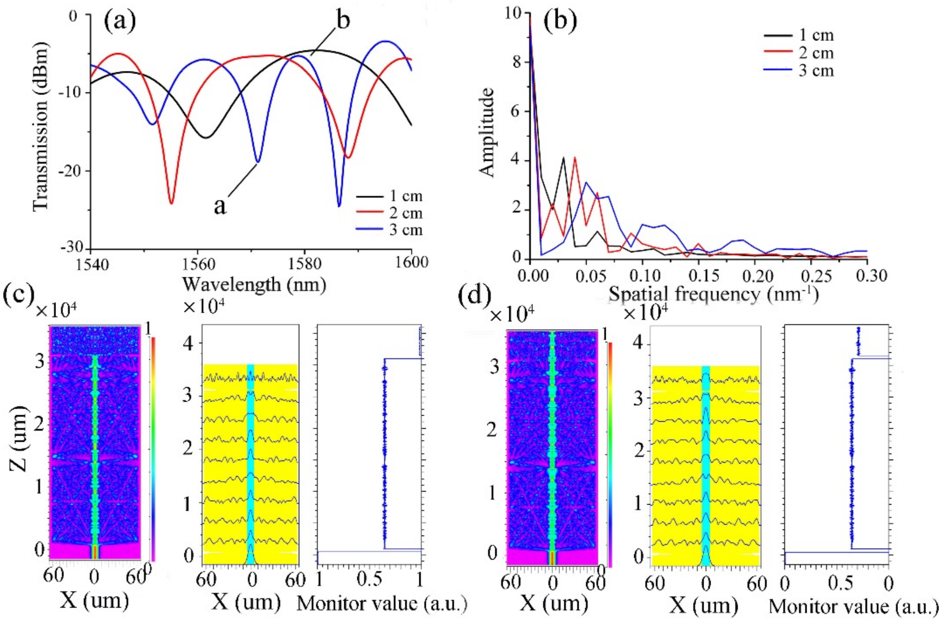

Figure 2. (**a**) The simulated spectral response of fiber MZI with arm length L of 1, 2, and 3 cm respectively; (**b**) The corresponding spatial frequency; (**c**) and (**d**) The distributions of optical field and normalized optical intensity propagating along MZI with arm length of 3 cm at dip *a* 1571.2 nm and peak *b* 1578.8 nm.

3. Experiments and Results

3.1 MZI sensor

Manually operation of arc-discharge of the fusion splicer (Fujikura 80c) has been adopted in this study to fabricate two micro tapers in a single SMF (G652D) as show in Fig. 3(a). Firstly, the jacket at the middle of the SMF was removed, and both ends of the optical fiber were fixed on the fusion splicer by two fiber clamps, where multiple arc-discharges were applied to the bare fiber and the fiber was pulled during the discharge. The size of micro taper fiber (taper transition length and taper waist diameter) can be controlled with precise control of arc-discharged time, power and pulling step length. In our experiments, the arc-discharged time and power are set to 200 ms and 50 bit respectively, and the step length was set to 500 μm. Figure 3(b) shows a microphotograph of the micro taper fiber made by the above method and parameters. An optical fiber MZI sensor can be fabricated by cascade two micro taper fibers as shown in Fig. 1. Figure 3(c), (d) and (e) show the transmission spectra of the fabricated fiber MZI with length *L* of 1, 2 and 3 cm respectively, at fixed temperature of 30 °C. One can see that as the *L* increases, the intensity of interference dips increases. The corresponding Fourier space spectrum was obtained by fast Fourier transform (FFT) of transmission spectrum. The spatial spectrogram with length *L* of 1, 2, and 3 cm are shown in Fig. 3(e). There is also only a main peak in Fourier spectrum. The spatial frequency of main peaks with *L*=1, 2, and 3 cm agrees well with that of the simulation results. We also consider the influence of waist diameter *D* on the extinction ratio of the structure. Figure 3(f) shows the measured Fourier space spectra with waist diameter of *D* = 50, 60, and 80 μm respectively. According to the experimental results, with the same length *L*, the maximum amplitude of main peak is observed for the structure with *D* = 80 μm, where the extinction ratio of over 10 dB with *D* = 80 μm were observed in Figs. 3(c-e).

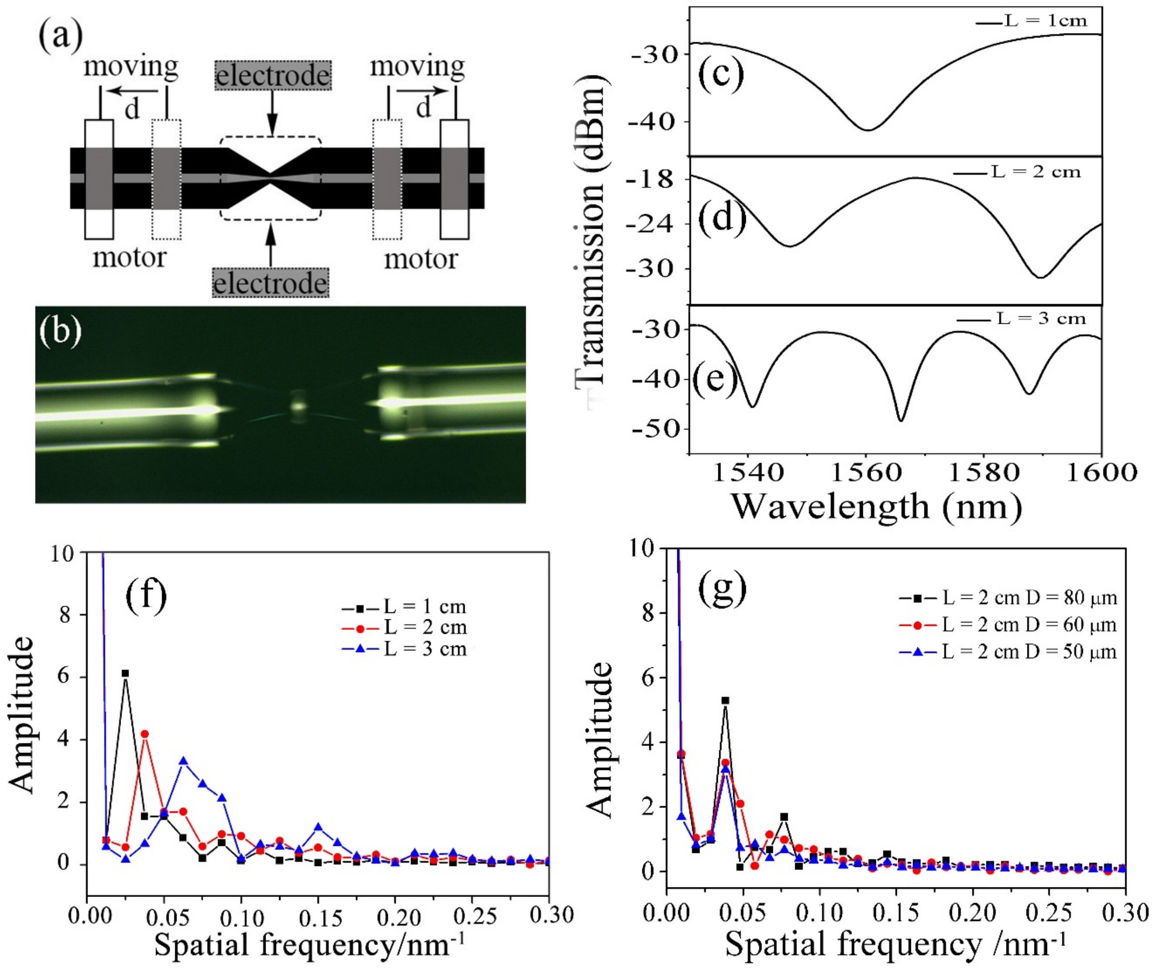

Figure 3. (**a**) Schematic diagram of micro taper structure fabrication process; (**b**) the photo under microscope; (**c**), (**d**) and (**e**) the spectral responses with sandwiched SMF length of 1, 2 and 3 cm respectively; (**f**) the FFT spatial frequency spectra with arm length of 1, 2, and 3 cm respectively. (**g**) The FFT spatial frequency spectra with waist diameter of 50, 60, and 80 μm, respectively.

Figure 4 shows the experimental setup for temperature, strain and RI measurements. The transmission spectra of the sensors were measured by usinging an SC-5-FC broadband light source (BBS) as an optical source, and an optical spectrum analyzer (OSA, AQ6370) as a demodulation equipment. In addition, the MZI sensor with sandwiched SMF length of about *L*=3 cm was selected for testing. Since the furnace used as heat source in our experimental setup has a heat channel with heating length up to 20 cm, it is believed that the furnace can provide a uniform temperature distribution for our sensor with sensor length of circa 3 cm.

The temperature response of the sensor was investigated without annealing firstly. As can be seen from Fig. 5(a), as the temperature increased from 100 °C to 950 °C, the spectral dip wavelength shifted to longer wavelength and vice versa. However, the wavelength shift during cooling does not match with that of increasing temperature. This result indicates that the sensor isn't stable within the temperature measurement range. Therefore, an annealing process on the sensor was applied to the sensor at high temperature of 1000 °C for three hours, as shown in Figure 5(b). And then, we use the annealed sensor to study the high-temperature sensing characteristics, from 80 °C to 950 °C, as shown in Fig. 5(c). The results show that the wavelength shifts for both heating and cooling overlapped well with sensitivity of 0.114 nm/°C and 0.116 nm/°C respectively, indicating that the sensor has stable temperature measurements. After two days, we also performed a repetitive experiment and the result overlapped well with the previous results with sensitivity of 0.111 nm/°C, which is consistent with the previous one, as show in Fig. 5(c).

Since the most common cross-sensitivity is caused by surrounding RI and strain applied to the sensor, the influence of RI and strain on the sensor's spectral response was investigated as shown in Fig. 6. Figure 6(a) show that the sensor has RI sensitivity of 5.128 nm/RIU and Fig. 6(b) show that the sensor has strain sensitivity of 1.33 pm/με. Since the surrounding air of the sensor has very low RI variation to temperature, for example, at normal pressure, the refractive index of air are 1.00027 and 1.00029 at 0 °C and 20 °C respectively, which has only 2×10^{-5} RI variations, the RI induced wavelength shift is negligible. Hence the air induced RI variations has limited influence on the measurement accuracy for the temperature sensor. However the temperature is sensitive to strain, which is a disadvantage of this type of sensor.

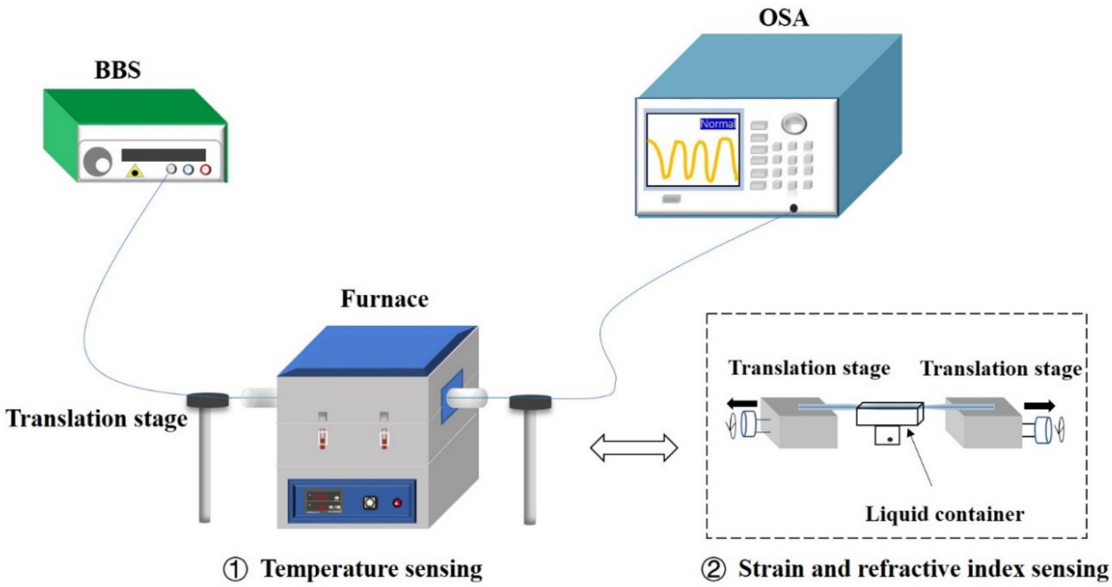

Figure 4. Schematic diagram of experimental setup for temperature, strain and RI measurements.

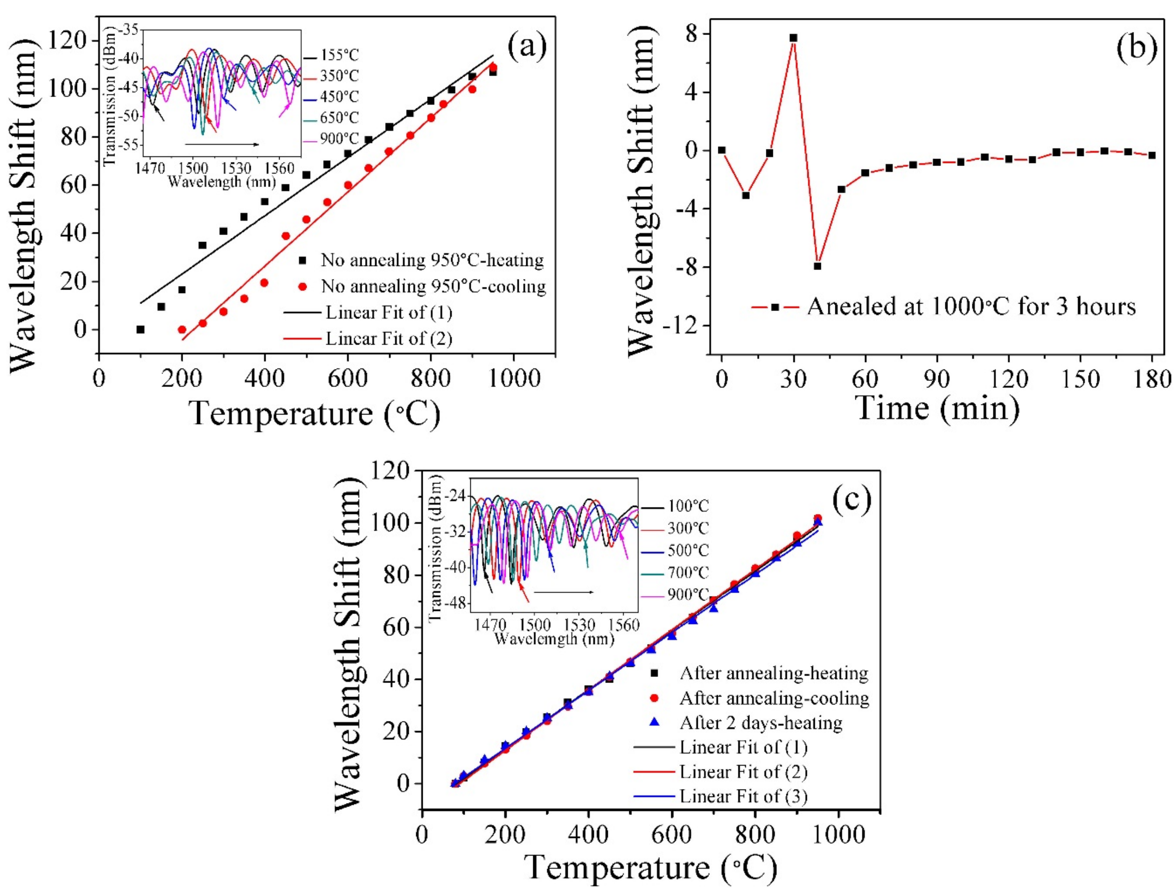

Figure 5. Wavelength shift versus temperature for MZI based sensor (L = 3 cm): (**a**) Wavelength shift of a sensor with no -annealing process. (**b**) The corresponding stability test in 3 hours before and after annealing process at 1000 °C. (**c**) The same dip was chosen for annealing processes and in the inset an example of the temperature shifting of the sensor after annealing at 1000 °C for 3 hours.

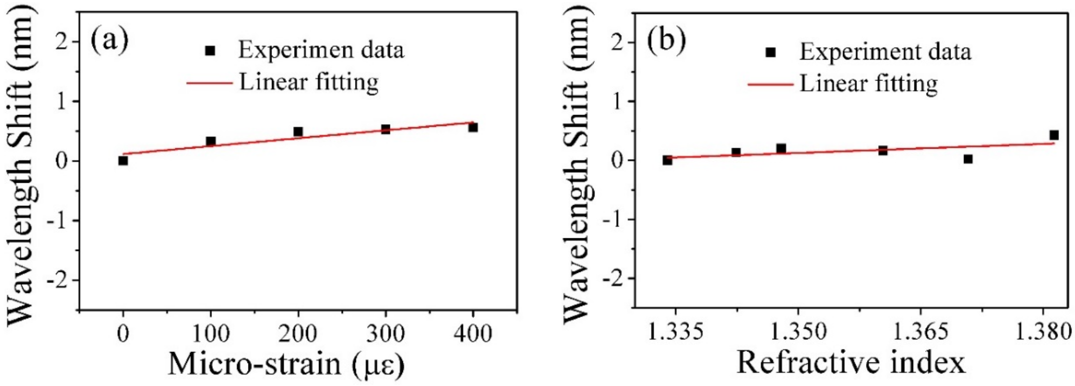

Figure 6. (**a**) Relationship between Micro-stain and wavelength. (b) Relationship between RI and wavelength

3.2 MZI Probe

In real application, it is more convenient to use a probe-type sensor structure. The sensor fabrication method is similar as that illustrated in Section 3.1. The only difference is that only one micro taper is fabricated and the sandwiched SMF was cut smoothly using a cleaver. A schematic diagram of MZI probe based on the micro-fiber taper is shown in Fig. 7(a). The Experimental setup of temperature measurement with the probe-type MZI is shown in Figure. 7(b). The incident light travels through the circulator to the sensor probe. At the end of the fiber sensor probe, due to the Fresnel reflection, the reflected light passes through the circulator again, and detected by an OSA. The advantage of the probe structure is that it can be inserted directly into the object or solution to be tested without being affected by strain. Four MZI probes were made and the effects of the interference arms on the performance of the sensor probe were investigated using different arm lengths *B* = 1, 1.5, 2 and 3 cm respectively. The diameter and micro taper length of the sensor were *A* = 80 μm, *b* = 500 μm respectively. The corresponding transmission spectra are shown in Figs. 8(a) - (d). respectively. As the length of *B* increases, the fringe-free spectral range (FSR) decreases, and the extinction ratio of all probes also exceeds 10 dB.

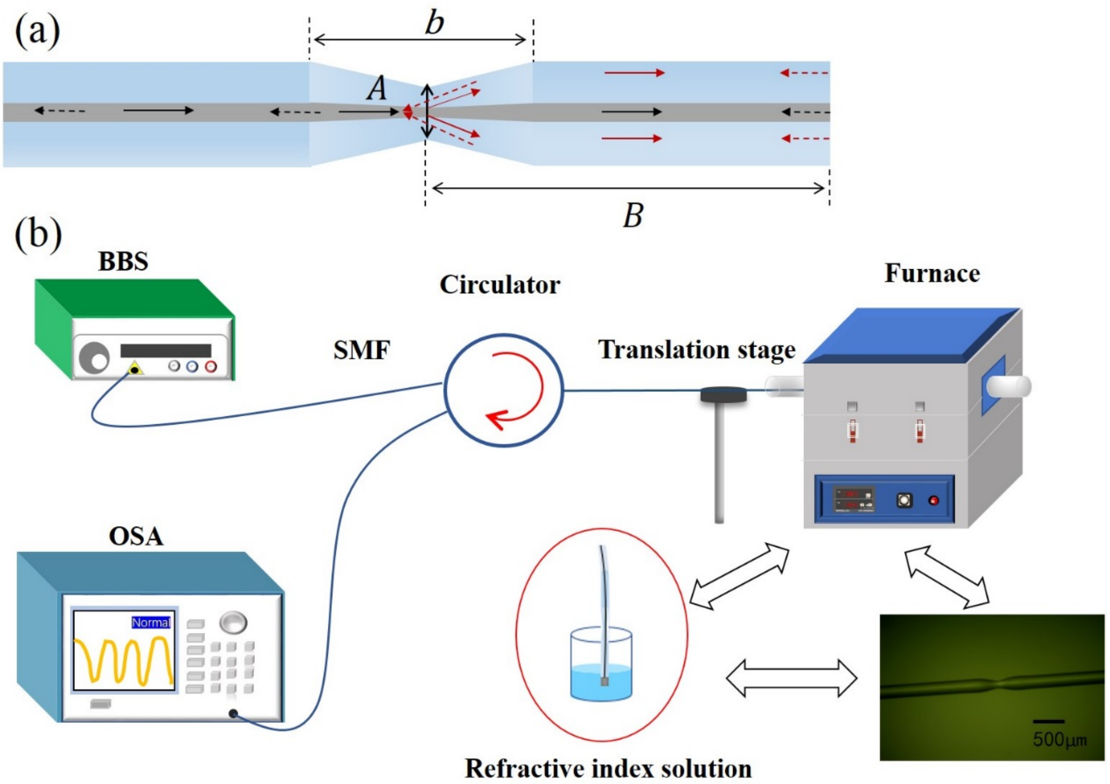

Figure 7. (**a**) Schematic diagram of the probe-type MZI. (**b**) Experimental setup. Inset figure is the optical microscope image of the probe-type MZI. BBS: Broadband Source, OSA: Optical Spectrum Analyzer, SMF: Single Mode Fiber.

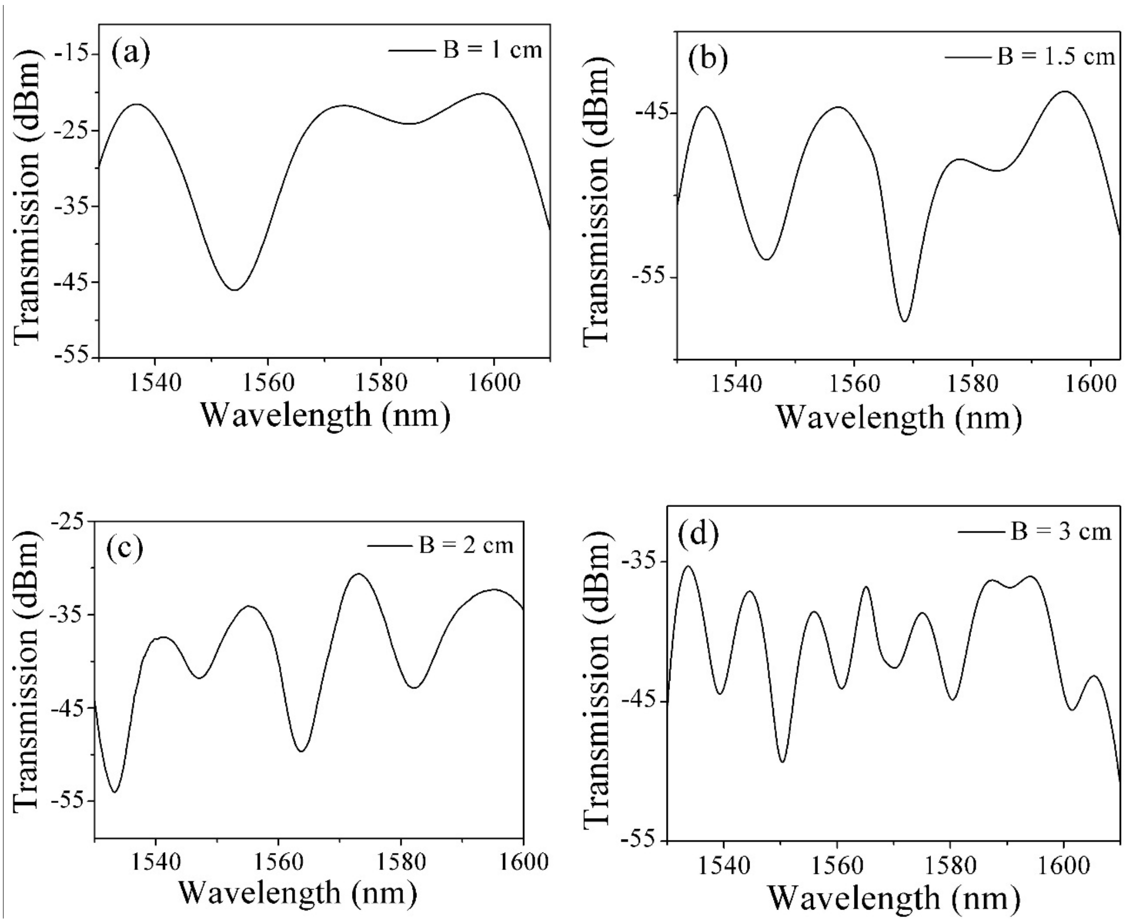

Figure 8. The transmission spectra of the proposed probe-type MZI with different *B* (interference length), (**a**), (**b**), (**c**), and (**d**) are 1, 1.5, 2, and 3 cm, respectively.

A probe-type MZI with lengths *B* of 2 cm were selected to test temperature response. As can be seen from Fig. 9(a), we measured the stability of the sensor at a constant temperature (200 ° C, 500 ° C and 950 ° C), each for 30 mins. As shown in Fig. 9(a), the sensor has a wavelength shift of less than 0.3 nm at 200 ° C and 500 ° C, indicating that good stability of the sensor. However, when the temperature increases to 950 ° C, the wavelength has a significant blue shift of 13.13 nm within 30 mins, indicating that sensor isn't suitable for high temperature measurements. This problem can be addressed by an annealing process [29]. In our experiments, an annealing process at 950 ° C for 2 hours has been conducted. It can be clearly seen that the wavelength has very small shifts (< 0.3 nm) at 950 ° C after annealing. The temperature response of the sensor after annealing is shown in Fig. 9(b) with temperature varies from 89 °C to 950 °C. There are three measured curves in Fig. 9(b), namely the heating and cooling circle, and the heating circle after 2 days. Linear fitting to the three measurement results have been conducted and the results show that temperature sensitivity of the three linear fit are the same of 0.11 nm / °C, which is ten times as that of traditional FBG and single-mode multimode single-mode fiber [35]. The correlation coefficient R^2 of the linear fitting curves are 0.99433, 0.99388 and 0.99211 respectively, showing good linearity of the results.

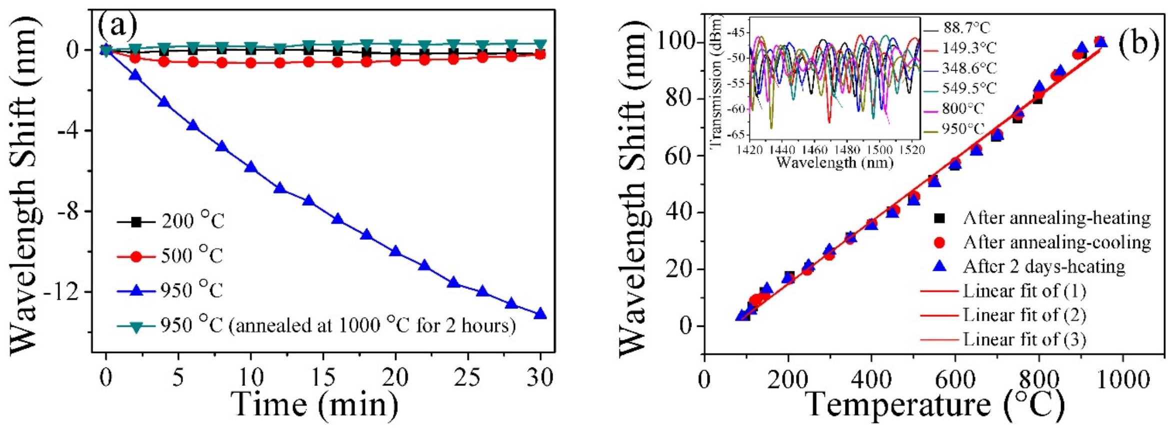

Figure 9. **(a)** Probe-type MZI based sensor (B = 2 cm) stability test (b) wavelength shift of the sensor during heating and cooling of the after annealing and inset figure is the temperature response of interference spectra from 89 °C to 950 °C.

4. Conclusions

In this work, a novel micro taper in-line fiber MZI structure for temperature measurement was proposed and studied in both simulation and experiments. The sensor has a maximum temperature sensitivity of 0.116 nm/°C with good stability at 950 °C after proper annealing process. The influence of surrounding RI and strain applied to the sensor was investigated and the results demonstrated that the temperature sensitivity is independent to surrounding RI but sensitive to strain. An improved probe-type fiber MZI was proposed and experimentally investigated to overcome the strain sensitivity. The MZI probe after annealing process has temperature sensitivity as high as 0.11 nm/°C over a wide temperature range from 89 °C ~950 °C with good stability. The proposed in-line fiber MZI temperature sensor has the advantages of good reproducibility, simple manufacture, compact structure and wide measurement range.

Funding: This research was funded by the National Natural Science Foundations of China (Grant No.11864025 and 61665007), Jiangxi provincial department of education science and technology project (Grant No. GJJ170609), and Nanchang Hangkong University graduate student innovation special fund project (Grant No. YC2018-S378), State Key Laboratory of Advanced Optical Communication Systems and Networks, Shanghai Jiao Tong University, China.

Conflicts of Interest: The authors declare no conflict of interest.

References

1. Wang Y. Review of long period fiber gratings written by CO2 laser[J]. Journal of Applied Physics, 2010, 108(8):11-279.
2. Rao Y J, Webb D J, Jackson D A, Zhang L, Bennion I. High-resolution, wavelength-divisionmultiplexed in-fibre Bragg grating sensor system [J]. Electronics Letters, 1996, 32(10): 924-926.
3. Wang Y P. Review of long period fiber gratings written by CO2 laser [J]. Journal of Applied Physics, 2010, 108(8): 081101-1-081101-18.
4. Lee B H, Kim Y H, Park K S, Eom J B, Kim M J, Rho B S, Choi H Y. Interferometric fiber optic sensors [J]. Sensors, 2012, 12(3): 2467-2486.
5. Zhu T, Wu D, Liu M, Duan D W. In-line fiber optic interferometric sensors in single-mode fibers [J]. Sensors, 2012, 12(8): 10430-10449.
6. Wei T, Han Y, Tsai H L, Xiao H. Miniaturized fiber inline Fabry-Perot interferometer fabricated with a femtosecond laser [J]. Optics Letters, 2008, 33(6): 536-538.
7. Lee C L, Ho H Y, Gu J H, Yeh T Y, Tseng C H. Dual hollow core fiber-based Fabry-Perot interferometer for measuring the thermo-optic coefficients of liquids [J]. Optics Letters, 2015, 40(4): 459-462.
8. Liu S, Wang Y P, Liao C R, Wang G J, Li Z Y, Wang Q, Zhou J T, Yang K M, Zhong X Y, Zhao J, Tang J. High-sensitivity strain sensor based on in-fiber improved Fabry-Perot interferometer [J]. Optics Letters, 2014, 39(7): 2121-2124.
9. Li Z Y, Liao C R, Wang Y P, Xu L, Wang D N, Dong X P, Liu S, Wang Q, Yang K M, Zhou J T. Highly-sensitive gas pressure sensor using twin-core fiber based in-line Mach-Zehnder interferometer [J]. Optics Express, 2015, 23(5): 6673-6678.
10. Li Z Y, Liao C R, Song J, Wang Y, Zhu F, Dong X P. Ultrasensitive magnetic field sensor based on an in-fiber Mach-Zehnder interferometer with a magnetic fluid component [J]. Photonics Research, 2016, 4(5): 197-201.
11. Wang, P., et al., Methylcellulose coated humidity sensor based on Michelson interferometer with thin-core fiber. Sensors and Actuators A: Physical, 2019. 288: p. 75-78.
12. S. Zhang, Y. Liu, H. Guo, A. Zhou and L. Yuan, "Highly Sensitive Vector Curvature Sensor Based on Two Juxtaposed Fiber Michelson Interferometers With Vernier-Like Effect," in *IEEE Sensors Journal*, vol. 19, no. 6, pp. 2148-2154, 15 March15, 2019.
13. Xiao, S., et al., Strain and temperature discrimination using two sections of PMF in Sagnac interferometer. Optics & Laser Technology, 2019. 113: p. 394-398.
14. Wu, B., et al., Optical fiber hydrogen sensor with single Sagnac interferometer loop based on vernier effect. Sensors and Actuators B: Chemical, 2018. 255: p. 3011-3016.
15. Wang, X. and Q. Wang, A High-Birefringence Microfiber Sagnac-Interferometer Biosensor Based on the Vernier Effect. Sensors, 2018. 18(12): p. 4114.
16. Tian Z, Yam S H, Barnes J, et al. Refractive Index Sensing With Mach–Zehnder Interferometer Based on Concatenating Two Single-Mode Fiber Tapers[J]. IEEE Photonics Technology Letters, 2008, 20(8):626-628.
17. Tian Z and Yam S H. In-line abrupt taper optical fiber Mach-Zehnder interferometric strain sensor[J]. IEEE Photonics Technology Letters, 2009, 21(3):161-163.
18. Lu P, Men L, Sooley K, et al. Tapered fiber Mach–Zehnder interferometer for simultaneous measurement of refractive index and temperature[J]. Applied Physics Letters, 2009, 94.
19. Wu D, Zhu T, Deng M, et al. Refractive index sensing based on Mach-Zehnder interferometer formed by three cascaded single-mode fiber tapers. [J]. Applied Optics, 2011, 50(11):1548.
20. Zhang S, Zhang W, Gao S, Geng P, and Xue X. Fiber-optic bending vector sensor based on Mach-Zehnder interferometer exploiting lateral-offset and up-taper[J]. Optics Letter, 2012, 37: 4480–4482.
21. Li L, Xia L, Xie Z, and Liu D. All-fiber Mach-Zehnder interferometers for sensing applications[J]. Optics Express, 2012, 20(10): 11109–11120.
22. Nguyen L V, Hwang D, Moon S, Moon D S, and Chung Y. High temperature fiber sensor with high sensitivity based on core diameter mismatch[J]. Optics Express, 2008, 16(15): 11369–11375.

23. Zhao N, Lin Q, Jing W, Jiang Z, Wu Z, Yao K, Tian B, Zhang Z, and Shi P. High temperature high sensitivity Mach–Zehnder interferometer based on waist-enlarged fiber bitapers[J]. Sens. Actuators A Phys., 2017, 267: 491–495.
24. Wu Q, Semenova Y, Wang P, et al. High sensitivity SMS fiber structure base refractometer – analysis and experiment[J]. oe/19/9/oe-19-9-7937.pdf, 2011, 19(9):7937-0.
25. Wu C, Fu H Y, Qureshi K K, et al. High-pressure and high-temperature characteristics of a Fabry-Perot interferometer based on photonic crystal fiber[J]. Optics Letters, 2011, 36(3):412-414.
26. Wu J, Miao Y, Song B, et al. Simultaneous measurement of displacement and temperature based on thin-core fiber modal interferometer[J]. Optics Communications, 2015, 340:136-140.
27. Wu Q, Semenova Y, Wang P, Farrell G, A comprehensive analysis verified by experiment of a refractometer based on an SMF28- Small-Core Singlemode fiber (SCSMF) -SMF28 fiber structure[J], Journal of Optics, 2011, 13(12): 125401.
28. Gu B, Yin M J, Zhang A P, et al. Low-cost high-performance fiber-optic pH sensor based on thin-core fiber modal interferometer. [J]. Optics Express, 2009, 17(25):22296.
29. Liu D, Wu Q, Mei C, et al. Hollow Core Fiber Based Interferometer for High-Temperature (1000 °C) Measurement[J]. Journal of Lightwave Technology, 2018, 36(9):1583-1590.
30. Li Y, Liu Z, Jian S. Multimode interference refractive index sensor based on coreless fiber[J]. Photonic Sensors, 2014, 4(1):21-27.
31. Antonio-Lopez J E, Eznaveh Z S, Likamwa P, et al. Multicore fiber sensor for high-temperature applications up to 1000°C[J]. Optics Letters, 2014, 39(15):4309.
32. Moon D S, Hwang D, Nguyen L V, et al. High temperature fiber sensor with high sensitivity based on core diameter mismatch[J]. Optics Express, 2008, 16(15):11369-11375.
33. Zhou S, Huang B, Shu X. A multi-core fiber based on interferometer for high temperature sensing[J]. Measurement Science and Technology, 2017, 28(4):045107.
34. Shao M, Qiao X, Fu H, et al. A Mach–Zehnder interferometric humidity sensor based on waist-enlarged tapers[J]. Optics and Lasers in Engineering, 2014, 52:86-90.
35. Wu Q, Hatta A M, Semenova Y, and Farrell G. Use of a SMS fiber filter for interrogating FBG strain sensors with dynamic temperature compensation[J]. Applied Optics, 2009, 48: 5451-5458.